Lattice dynamics of fluoride scheelites: I. Raman and infrared study of $LiYF_4$ and $LiLnF_4$ ($Ln = Ho, Er, Tm$ and Yb)

1997 J. Phys.: Condens. Matter 9 6941

(http://iopscience.iop.org/0953-8984/9/32/016)

J. Phys.: Condens. Matter **9** (1997) 6941–6956. Printed in the UK PII: S0953-8984(97)80394-3

Lattice dynamics of fluoride scheelites: I. Raman and infrared study of $LiYF_4$ and $LiLnF_4$ (Ln = Ho, Er, Tm and Yb)

S Salaün†, M T Fornoni†, A Bulou†, M Rousseau†, P Simon‡ and J Y Gesland†

† Laboratoire de Physique de l'Etat Condensé, Faculté des Sciences, Université du Maine, Avenue O Messiaen, 72017 Le Mans Cedex, France

‡ CRPHT, CNRS-1D, Avenue de la Recherche Scientifique, 45071 Orléans Cedex 02, France

Received 18 December 1996

Abstract. IR and Raman active modes have been measured in several fluoride scheelites, namely the laser matrix $LiYF_4$ (studied as a reference) and four $LiLnF_4$ compounds (Ln = Ho, Er, Tm and Yb). The observed phonons have been assigned in accordance with the various irreducible representations of the point group of the crystal. In $LiYF_4$ three modes never observed before have been measured. The polarized experimental IR reflection spectra have been analysed through a 'four-parameters' model to give the mode frequencies and dampings. For the whole set of the compounds, the frequency dependence of the dielectric function, optical indices and absorption coefficient have been deduced from the IR study. The electronic Raman effect has been shown in the low-temperature Raman spectra for Ln = Tm, Ho and Yb. The corresponding measured wavenumbers are compared with the calculated energies between crystal-field levels of LSJ states, each being associated to an irreducible representation of the ion-site group S_4.

1. Introduction

Lanthanide trifluorides (LnF_3), from europium ($Z = 63$) to lutetium ($Z = 71$), combine with lithium fluoride (LiF) to form an intermediate compound with a scheelite structure of general formula $LiLnF_4$ [1, 2]. $LiYF_4$ is generally associated with this particular family since it is the first isomorphic fluoride which has been synthesized and studied [3]. All of these compounds, pure or doped, are optically transparent insulators which are of considerable interest in optical applications [4–10]. Nowadays $LiYF_4$ is the most-used fluoride laser host crystal, generally doped with trivalent rare-earth ions (Nd^{3+}, Eu^{3+}, ...) [10, 11] and, more recently, with uranium [12]. In 1990, 36 different lasers based on $LiYF_4$ crystals doped with rare-earth ions producing various radiations were already listed by Kaminskii [4] in a review article.

Many experimental data are already reported concerning Raman scattering in $LiYF_4$ and $LiLnF_4$ compounds, and infrared spectroscopy in $LiYF_4$ and $LiTmF_4$ [13–16]. However, the frequencies of several vibrational modes were still missing, because they were not observed or identified. Such data being necessary to predict the phonon spectrum of fluoride scheelites for the $LiYF_4$ compound will be reported in paper II. The present paper deals with Raman and infrared measurements in $LiYF_4$ (studied as a reference) and $LiLnF_4$ compounds, with Ln = Ho, Er, Tm and Yb (Z = 67–70 successively); electronic Raman lines have been observed in low-temperature $LiLnF_4$ Raman spectra for Ln = Tm, Ho and Yb.

0953-8984/97/326941+16$19.50

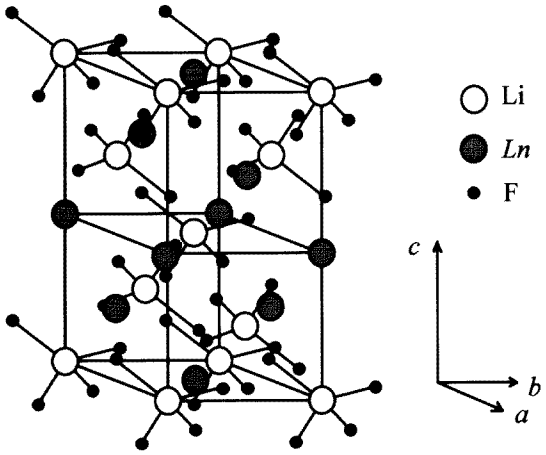

Figure 1. Tetragonal unit-cell of LiLnF$_4$ compounds (Ln = Ho, Er, Tm, Yb ; Y).

Table 1. Crystallographic parameters of LiYF$_4$ (Garcia *et al* [17]) and LiLnF$_4$ compounds (Landolt-Börnstein [18]), together with the ionic radius of the corresponding trivalent ion in a coordinance of eight fluorine ions (Kaminskii [4]).

	Compound				
	LiYF$_4$	LiHoF$_4$	LiErF$_4$	LiTmF$_4$	LiYbF$_4$
a (Å)	5.164	5.175	5.162	5.145	5.132
c (Å)	10.741	10.75	10.70	10.64	10.59
c/a	2.080	2.078	2.073	2.067	2.064
Ln^{3+} (Å)	1.16	1.16	1.14	1.13	1.12

Section 2 reports on the results of a group theory analysis for zone-centre phonons in scheelite compounds, followed by discussions on the Raman and infrared results in sections 3 and 4 respectively. The experimental data have been analysed to yield the effective charges, the frequency dependence of the optical indices, and information about the atomic movements under some of the vibrational modes is given.

2. Structure and dynamics

LiYF$_4$ and LiLnF$_4$ compounds crystallise with the scheelite structure [1–3, 17, 18]; hence, they belong to the $C_{4h}^6(I4_1/a)$ space group and are usually described by their body-centred tetragonal unit cell ($Z = 4$) (shown in figure 1). It must be noted that the Li and Ln atoms occupy a $\bar{4}$-symmetry site while the fluorine ions lie in a general symmetry, so that none of them are on an inversion centre. The crystallographic parameters a and c given in the literature are reported in table 1. Note that there is a linear relation between the ratio c/a and the Ln^{3+} ionic radii [4, 19].

The samples used throughout this work have been grown by J Y Gesland†, using the

† Université du Maine-Cristallogénèse (UMC), Laboratoire PEC, Faculté des Sciences, Université du Maine, Avenue O Messiaen, 72017 Le Mans Cedex, France

Czochralski technique. The single crystals were Laue oriented and cut perpendicularly to the crystallographic axes, to obtain rectangular parallelepipeds of about $5 \times 5 \times 10$ mm^3 volume, the *c*-axis being parallel to the 1 cm edge. Faces have been polished for good optical quality.

The scheelite primitive cell (trigonal) containing two Li*Ln*F$_4$ units, has 36 degrees of freedom (including rigid translation) per wavevector. The 36 vibrational modes at the centre of the Brillouin zone are distributed among the irreducible representations of C_{4h} as follows [20]:

$$\Gamma^{\text{vib}} = 3A_g + 5B_g + 5E_g + 5A_u + 3B_u + 5E_u.$$

One A_u and one E_u mode corresponds to rigid translations of the whole crystal. The other A_u and E_u modes are infrared active with a dipole moment respectively parallel with, and perpendicular to the crystalline axis *c*. The g modes are Raman active and correspond to the following components of the Raman polarizability tensor:

$$A_g : \alpha_{xx} + \alpha_{yy}; \alpha_{zz}$$
$$B_g : \alpha_{xx} - \alpha_{yy}; \alpha_{xy}$$
$$E_g : \alpha_{zx}, \alpha_{yz}.$$

The phonons of B_u symmetry are neither Raman nor infrared active.

A more complete group theory analysis has been performed in order to know the symmetry-adapted motions, summarized in table 2, of each atom in the primitive cell (their reduced coordinates are brought to your attention in table 2). It appears that only the fluorine atoms may move under A_g and B_u modes; Li and *Ln* atoms move in the (001) plane for E_g and E_u modes (doubly degenerated), and along the four-fold axis *c* for B_g and A_u symmetries.

3. Raman spectroscopy

Among all the compounds studied in this work, only LiYF$_4$ is diamagnetic and its ground state corresponds to the $^1S_0$ term. Thus, the experimental investigations of the vibrational properties of this particular compound cannot be perturbed by fluorescence lines nor by the electronic Raman effect, apart from an eventual small amount of lanthanide impurities, but which would be of poor intensity. LiYF$_4$ is therefore considered as a reference for the Raman study of the isomorphic Li*Ln*F$_4$ compounds where the electronic level schemes are more complicated and where the ground states are degenerate: the interpretation of corresponding Raman spectra requires a comparison with LiYF$_4$ ones.

3.1. Experimental equipment

The Raman spectra were recorded with a Dilor Z24 triple monochromator, equipped with a cooled photomultiplier. A Leybold cryogenerator was used to obtain low temperatures. Following Porto [21], the scattering geometry is denoted by symbols such as $x(zz)y$, which means that the laser light enters along the crystalline *x* axis, the scattered light is observed along the *y* axis, and the incident and scattered polarizations select the zz component of the Raman polarizability tensor (the *x*, *y* and *z* axes are respectively parallel to the crystallographic axes *a*, *b* and *c*).

Table 2. Symmetry-adapted displacements for zone-centre phonons in the scheelite structure along a, b and c axes (first, second and third line, respectively). We only considered the atoms in the primitive cell of which reduced coordinates are given in the crystallographic basis $(\boldsymbol{a}, \boldsymbol{b}, \boldsymbol{c})$. E_g and E_u modes are doubly degenerated: the second eigenvector is obtained by complex conjugation (*) of the first one. a_i, b_i and c_i coefficients may be complex.

Atom (no.) (reduced coordinates)	A_g	B_g	E_g		A_u	B_u	E_u	
Li (1)	0	0	a_1		0	0	a_1	
(0, 0, 0)	0	0	$-\mathrm{i}a_1$	*	0	0	$\mathrm{i}a_1$	*
	0	c_1	0		c_1	0	0	
Li (2)	0	0	$-a_1$		0	0	a_1	
$(0, \frac{1}{2}, \frac{1}{4})$	0	0	$\mathrm{i}a_1$	*	0	0	$\mathrm{i}a_1$	*
	0	$-c_1$	0		c_1	0	0	
Y or *Ln* (3)	0	0	a_2		0	0	a_2	
$(0, 0, \frac{1}{2})$	0	0	$-\mathrm{i}a_2$	*	0	0	$\mathrm{i}a_2$	*
	0	c_2	0		c_2	0	0	
Y or *Ln* (4)	0	0	$-a_2$		0	0	a_2	
$(0, \frac{1}{2}, \frac{3}{4})$	0	0	$\mathrm{i}a_2$	*	0	0	$\mathrm{i}a_2$	*
	0	$-c_2$	0		c_2	0	0	
F (5)	a_1	a_3	a_3		a_3	a_3	a_3	
(x, y, z)	b_1	b_3	b_3	*	b_3	b_3	b_3	*
	c_1	c_3	c_3		c_3	c_3	c_3	
F (6)	$-a_1$	$-a_3$	a_3		$-a_3$	$-a_3$	a_3	
$(-x, -y, z)$	$-b_1$	$-b_3$	b_3	*	$-b_3$	$-b_3$	b_3	*
	c_1	c_3	$-c_3$		c_3	c_3	$-c_3$	
F (7)	$-b_1$	b_3	$\mathrm{i}b_3$		b_3	$-b_3$	$-\mathrm{i}b_3$	
$(-y, x, -z)$	a_1	$-a_3$	$-\mathrm{i}a_3$	*	$-a_3$	a_3	$\mathrm{i}a_3$	*
	c_1	c_3	$\mathrm{i}c_3$		c_3	$-c_3$	$-\mathrm{i}c_3$	
F (8)	b_1	$-b_3$	$\mathrm{i}b_3$		$-b_3$	b_3	$-\mathrm{i}b_3$	
$(y, -x, -z)$	$-a_1$	a_3	$-\mathrm{i}a_3$	*	a_3	$-a_3$	$\mathrm{i}a_3$	*
	$-c_1$	c_3	$-\mathrm{i}c_3$		c_3	$-c_3$	$\mathrm{i}c_3$	
F (9)	a_1	a_3	$-a_3$		$-a_3$	$-a_3$	a_3	
$(x, y + \frac{1}{2}, \frac{1}{4} - z)$	b_1	b_3	$-b_3$	*	$-b_3$	$-b_3$	b_3	*
	$-c_1$	$-c_3$	c_3		c_3	c_3	$-c_3$	
F (10)	$-a_1$	$-a_3$	$-a_3$		a_3	a_3	a_3	
$(-x, \frac{1}{2} - y, \frac{1}{4} - z)$	$-b_1$	$-b_3$	$-b_3$	*	b_3	b_3	b_3	*
	$-c_1$	$-c_3$	$-c_3$		c_3	c_3	c_3	
F (11)	$-b_1$	b_3	$-\mathrm{i}b_3$		$-b_3$	b_3	$-\mathrm{i}b_3$	
$(-y, x + \frac{1}{2}, \frac{1}{4} + z)$	a_1	$-a_3$	$\mathrm{i}a_3$	*	a_3	$-a_3$	$\mathrm{i}a_3$	*
	c_1	$-c_3$	$\mathrm{i}c_3$		c_3	$-c_3$	$\mathrm{i}c_3$	
F (12)	b_1	$-b_3$	$-\mathrm{i}b_3$		b_3	$-b_3$	$-\mathrm{i}b_3$	
$(y, \frac{1}{2} - x, \frac{1}{4} + z)$	$-a_1$	a_3	$\mathrm{i}a_3$	*	$-a_3$	a_3	$\mathrm{i}a_3$	*
	c_1	$-c_3$	$-\mathrm{i}c_3$		c_3	$-c_3$	$-\mathrm{i}c_3$	

3.2. Results in $LiYF_4$

Raman spectra were recorded with 250 μm slit-width (spectral resolution ≈ 2.5 cm^{-1}) and a typical laser power of 100 mW. The use of various excitations† (514.5, 496.5, 488 and 457.9 nm) guarantees that all the lines must be attributed to Raman scattering, consistent with the lack of luminescence expected in this compound.

† The excitation must be carefully selected in the case of the other Li*Ln*F_4 compounds because of possible fluorescence.

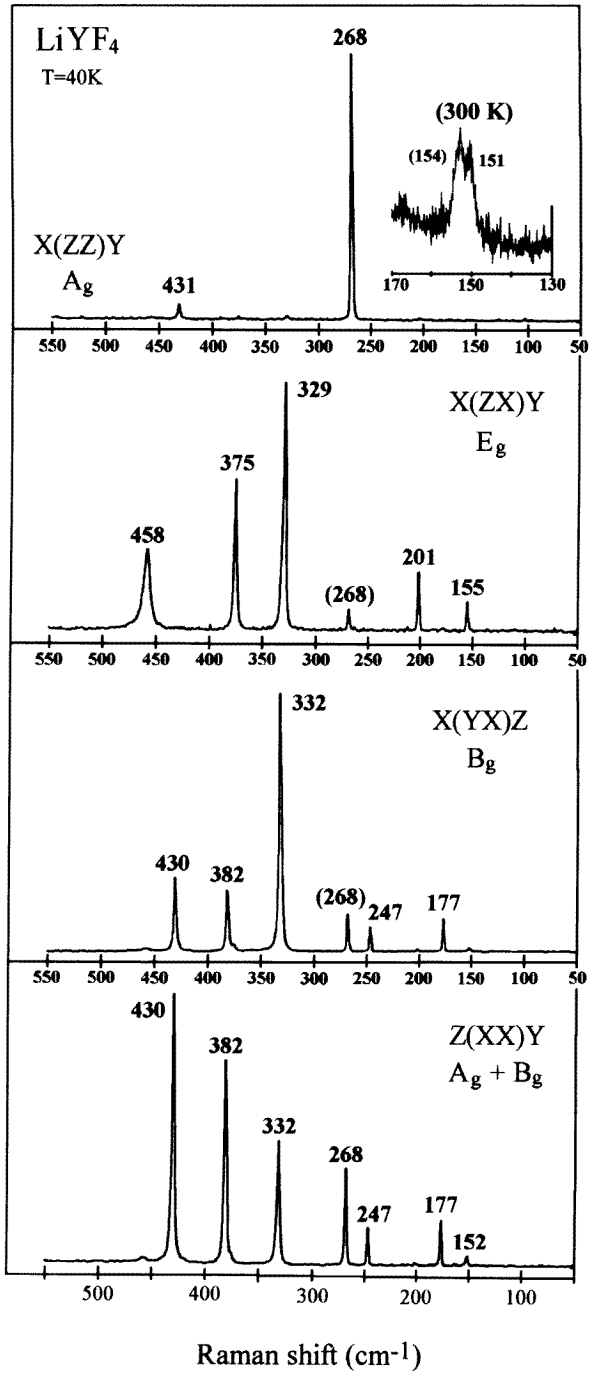

Figure 2. Experimental Raman spectra recorded at 40 K in $LiYF_4$. The geometries of the theoretically Raman-active modes are indicated for each scattering geometry. When a peak is attributed to a contamination by an intense line active in another geometry, its position (given in cm^{-1}) appears in parentheses. The inset shows the accumulation of 10 spectra (recorded at room temperature) realized to show the lowest-frequency A_g mode.

Table 3. Experimental Raman active phonon frequencies in $LiYF_4$.

T (K)	$A_g(cm^{-1})$		$E_g(cm^{-1})$					$B_g(cm^{-1})$					Reference
300	151	265 427	154	199	326	373	447	174	246	327	379	427	This
40	152	268 431	155	201	329	375	458	177	247	332	382	430	work
300	—	269 430	158	203	329	376	450	177	251	331	382	426	[16]
4.2	—	273 434	160	207	334	379	462	182	252	336	385	432	
300	—	264 425	153	199	329	368	446	177	248	329	382	427	[13]

Figure 2 shows the Raman spectra collected at 40 K, with an excitation at 496.5 nm, for different scattering geometries. It can be noted that the lowest frequency A_g mode (at 152 cm^{-1}) has been evidenced for the first time. While it appears clearly in the $Z(XX)Y$ spectra, the corresponding signal is very weak in the $X(ZZ)Y$ configuration and overlaps with polarization leaks of an E_g line (at 155 cm^{-1}), as shown on the inset in figure 2; an accumulation of 10 spectra, collected with an excitation of 488 nm, was necessary to evidence this peak at room temperature.

Table 3 lists the frequencies of the observed Raman-active phonons at room temperature and 40 K, assigned to the various irreducible representations of C_{4h}. They appear to be weakly temperature dependent. As a comparison, the results previously obtained by Miller *et al* [13] and Schulteiss *et al* [16] have also been reported in table 3. Then all the Raman-active symmetry predicted modes are unambiguously observed and assigned.

3.3. Results in $LiLnF_4$ compounds

In so far as Ln^{3+} ions have a lot of electronic levels between 12 500 and 25 000 cm^{-1}, the probability for the excitation to be close to an absorption band is large: luminescence lines may be induced. In order to avoid such an effect which may be much more intense than the Raman lines, the wavelength of the excitation must be carefully selected for each compound.

$LiHoF_4$: the best spectra are obtained with $\lambda_0 = 514.5$ or 496.5 nm. The 457.9 nm radiation generates a strong luminescence.

$LiErF_4$: only the 457.9 nm radiation gives rise to convenient spectra. With $\lambda_0 =$ 496.5 nm, one observes in the [0, 500 cm^{-1}] frequency range additional lines as intense as the Raman lines, and the use of $\lambda_0 = 514.5$ nm leads to broad luminescence bands.

$LiTmF_4$: any of the available argon-ion laser wavelengths can be used for this particular compound.

$LiYbF_4$: we recorded the Raman spectra with $\lambda_0 = 496.5$ and 514.5 nm. With $\lambda_0 = 457.9$ nm as excitation, Raman lines are superimposed to the luminescence bands (probably resulting from impurities).

As an illustration, we report in figure 3 the Raman spectra obtained at 40 K for the various configurations in $LiHoF_4$.

3.3.1. Vibrational Raman effect. The Raman spectra obtained, at room-temperature, for each compound within the experimental conditions described above, appear to be very similar. This may be attributed to the very small variation of mass and ionic radius from Ho^{3+} to Yb^{3+} in the lanthanide series. They are also extremely similar to the spectra of the

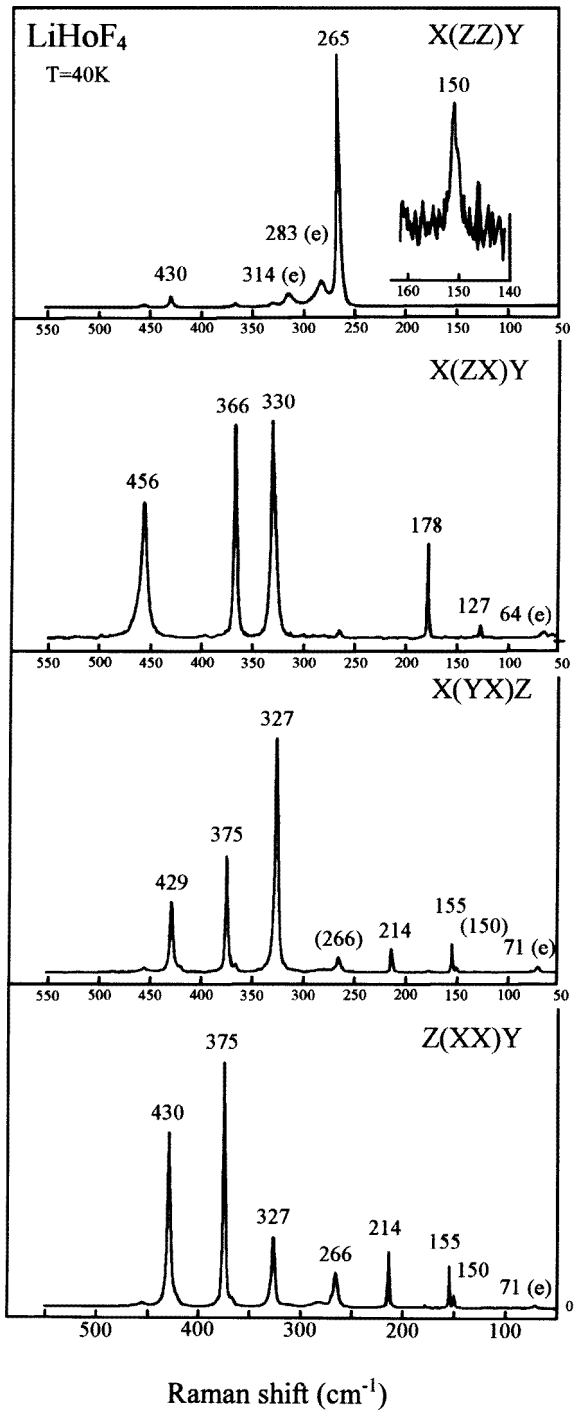

Figure 3. Experimental Raman spectra in $LiHoF_4$ recorded at 40 K in different scattering geometries. Electronic lines are indicated by e, and the frequencies (expressed in cm^{-1}) of lines attributed to polarization leaks are in parentheses.

Table 4. Raman active frequencies (in cm^{-1}) in LiLnF$_4$ compounds (Ln = Ho, Er, Tm, Yb; Y) at room temperature and 40 K (italics). A dash appears when the corresponding mode could not be evidenced experimentally, and an asterisk indicates that the softening on cooling may be attributed to an electron–phonon coupling [24].

	Compound				
	$LiYF_4$	$LiHoF_4$	$LiErF_4$	$LiTmF_4$	$LiYbF_4$
$A_g(cm^{-1})$	151/—	151/*150*	151/—	153/*153*	152/*152*
	265/*268*	269/*265*	270/*270*	270/*269*	269/*270*
	427/*431*	426/*430*	430/*434*	433/*438*	438/*441*
$B_g(cm^{-1})$	174/*177*	153/*155*	153/—	153/*156*	152/*152*
	246/*246*	214/*214*	215/—	216/*218*	216/*215*
	327/*332*	323/*327*	326/—	324/*301**	340/*351*
	380/*382*	373/*375*	378/—	383/*401*	392/*406*
	427/*430*	426/*429*	430/—	435/*438*	437/*441*
$E_g(cm^{-1})$	154/*155*	127/*127*	129/*129*	130/*130*	130/*131*
	199/*201*	177/*178*	179/*181*	181/*183*	182/*184*
	326/*329*	326/*330*	330/*334*	330/*319**	325/*316**
	373/*375*	365/*366*	368/*370*	371/*383*	371/*371*
	447/*458*	446/*456*	450/*459*	457/*469*	462/*479*

isomorphic compound $LiYF_4$ as shown by the comparison of figures 2 and 3. Therefore, as already mentioned, the mode assignments have been established on the basis of the $LiYF_4$ ones (table 2): resulting attributions are reported in table 4.

From room temperature down to 40 K, the line-widths decrease and the frequencies slightly increase, except for the modes identified by an asterisk in table 4. Their quite important decrease may be attributed to an electron–phonon coupling [24].

Concerning the dynamical properties, the main difference between $LiYF_4$ and LiLnF$_4$ crystals is the trivalent ion mass. The Ln^{3+} being about twice as heavy as Y^{3+}, the frequencies of modes that involve displacements of trivalent ions should significantly decrease from $LiYF_4$ to LiLnF$_4$. Such a shift is experimentally observed for the two low frequency E_g and B_g symmetry modes. This is consistent with the symmetry-adapted vectors reported in table 2 since, among the Raman-active modes, only those with E_g and B_g symmetries may imply lanthanide motions. It can also be deduced that the (heavy) lanthanide ions mostly vibrate at low frequencies.

Additionally, one may remark that, thanks to the 'red shift' of the low frequency E_g mode, the weak A_g line no longer overlaps with E_g (unlike in $LiYF_4$) in the $X(ZZ)Y$ configuration which makes the experimental results easier to interpret.

3.3.2. Electronic Raman effect. The Raman spectra of the LiLnF$_4$ compounds collected at 40 K exhibit extra sharp lines (see figure 3), with respect to those collected at room temperature. These lines are not dependent on the excitation wavelength and have been attributed to the electronic Raman effect.

The electronic configuration $Xe(4f)^n(5s)^2(5p)^6$ of Ln^{3+} ions (n = 1–14) gives rise to various LSJ manifolds, which are $(2J+1)$-fold degenerate. Each crystal-field level of such LSJ states ($^{2S+1}L_J$) is associated with an irreducible representation Γ_J of the ion-site group (or double-group when J is half-integer), i.e. S_4 for lanthanide ions in LiLnF$_4$ compounds.

Table 5. Calculated energies of the LSJ-multifold crystal-field levels for Ln^{3+} ions, selection rules and measured energies of electronic Raman lines for various scattering geometries in $LiLnF_4$ compounds (Ln = Tm, Ho, Yb).

			E_{meas}(cm^{-1})					
			This work				Kupchikov *et al* [22]	
E_{calc} (cm^{-1})	Γ	Selection rules (Raman)	ZZ	XX	XY	Christensen [5, 6]	77 K	2 K
$LiTmF_4$								
0	2							
31	3,4	YZ, ZX				32		
62	1	XY, XX		70	68	57	65	71
287	2	XX, ZZ	278					
316	2	XX, ZZ	319	319			317	319
365	1	XY, XX		364	364		359	363
382	3,4	YZ, ZX						
410	3,4	YZ, ZX						
421	1	XY, XX						
436	2	XX, ZZ						

$LiHoF_4$

			E_{meas}(cm^{-1}) (this work)			
			ZZ	XX	YX	ZX
0	3,4					
8	2	ZX, YZ				
20	2	ZX, YZ				
50	1	ZX, YZ				
59	1	ZX, YZ				58
72	3,4	ZZ, XX, XY		71	71	
211	1	ZX, YZ				
273	1	ZX, YZ				
275	3,4	ZZ, XX, XY	283	282	283	
284	2	ZX, YZ				
294	3,4	ZZ, XX, XY	314			
296	1	ZX, YZ				
310	2	ZX, YZ				

$LiYbF_4$

			E_{meas}(cm^{-1}) (this work)
			XY
0	7,8		
235	5,6	XX, XY, XZ, YZ	218
366	7,8	ZZ, XY, XZ, YZ	
456	5,6	XX, XY, XZ, YZ	

These ground states can be totally or partially split by the crystal field, with an overall separation smaller than 500 cm^{-1}. For the various Ln^{3+} ions studied in this work, the distributions of the corresponding Γ_J levels among the irreducible representations of the S_4

group are, using the notation of Koster *et al*:

$$\mathrm{Ho}^{3+}(4f^{10},\ ^{2S+1}L_J = {}^5I_8) : \Gamma_8 \rightarrow 5\Gamma_1 + 4\Gamma_2 + 4\Gamma_{3,4}$$
$$\mathrm{Er}^{3+}(4f^{11},\ {}^4I_{15/2}) : \Gamma_{15/2} \rightarrow 4\Gamma^*_{5,6} + 4\Gamma^*_{7,8}$$
$$\mathrm{Tm}^{3+}(4f^{12},\ {}^3H_6) : \Gamma_6 \rightarrow 3\Gamma_1 + 4\Gamma_2 + 3\Gamma_{3,4}$$
$$\mathrm{Yb}^{3+}(4f^{13},\ {}^2F_{7/2}) : \Gamma_{7/2} \rightarrow 2\Gamma^*_{5,6} + 2\Gamma^*_{7,8}.$$

The double subscripts imply degenerate one-dimensional representations: the physically irreducible representation is their direct sum. The levels associated with the double-valued representations, identified by asterisks, are Kramers doublets which may be split by application of a magnetic field (Zeeman–Raman effect).

Energies of each crystal-field levels of LSJ states have been calculated in LiLnF$_4$ compounds by Christensen [5, 6] for Ln = Ho, Er, Tm, and by Kupchikov [22] for ytterbium. If electronic Raman transitions are excited between the crystal-field levels of LSJ states, then the selection rules for such a process depends on integrals of the type $\langle\Psi_i|\alpha_{\mu\nu}|\Psi_f\rangle$, where α is the polarizability tensor and Ψ_i and Ψ_f refer to the wavefunctions of the initial (ground) and final state. The selection rules for S_4, obtained from the previous integral and tables of product representations, are given in [23]; we only report in table 5 the rules which may be applied in Raman spectroscopy.

Electronic Raman effect has been evidenced in low-temperature LiLnF$_4$ Raman spectra for Ln = Tm, Ho and Yb, but not in LiErF$_4$. The corresponding measured wavenumbers within different scattering geometries are reported in table 5 together with the calculated differences of energy between crystal-field levels of LSJ states, considering that only the lowest energy level is occupied at the investigated temperature (40 K). The selection rules are fulfilled. We bring to your attention also the results obtained by other authors, namely Christensen [5, 6] by infrared spectroscopy, and Kupchikov *et al* [22] by Raman spectroscopy.

4. Infrared-active modes

4.1. Experimental details

Room-temperature polarized reflection spectra were recorded with a Fourier-transform rapid-scan interferometer (BRUKER IFS 113C) at the CRPHT in Orléans (France). All of the experiments were performed at 6° from the normal incidence, in the spectral range 50–2000 cm^{-1}. The electric field vector of the incident beam was either perpendicular or parallel to the four-fold axis.

As shown in section 1, there are eight polar vibration modes, infrared active, in the scheelite structure, namely four polarized along the optical axis c (A_u modes), and four polarized perpendicularly to c (E_u modes). Room-temperature polarized reflection spectra obtained for LiYF$_4$ and LiLnF$_4$ compounds are shown on figure 4 (dotted curves). As expected, there are four bands for each polarization. These are grouped continuously between 180 and 500 cm^{-1} and their position is only slightly modified by the nature of Ln^{3+} ion, or by the substitution of a lanthanide ion to yttrium.

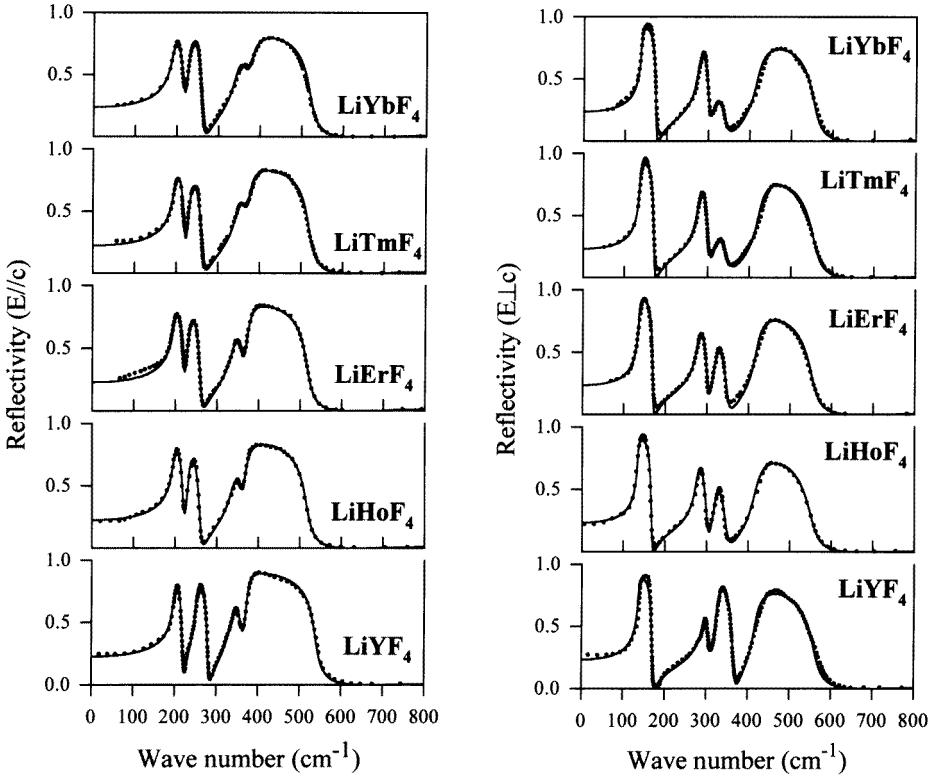

Figure 4. Room temperature reflection spectra in LiLnF$_4$ compounds (Ln = Ho, Er, Tm, Yb; Y). Experimental curves are drawn dotted and the full curves represent the result of an oscillator fit.

4.2. Analysis of experimental spectra

The measured reflectivity $R(\omega)$ of a material depends on the permittivity $\varepsilon(\omega)$ via Fresnel's formula in normal incidence:

$$R(\omega) = \left| \frac{\sqrt{\varepsilon(\omega)} - 1}{\sqrt{\varepsilon(\omega)} + 1} \right|^2 .$$

The solid curves in figure 4 are the results of an oscillator fit simulating the reflectance $R(\omega)$ through a dielectric function model, the factorized form of ε being convenient to represent even asymmetrical and wide bands:

$$\varepsilon(\omega) = \varepsilon' - \mathrm{i}\varepsilon'' = \varepsilon_\infty \prod_j \frac{\Omega_{j,\mathrm{LO}}^2 - \omega^2 + \mathrm{i}\gamma_{j,LO}\omega}{\Omega_{j,\mathrm{TO}}^2 - \omega^2 + \mathrm{i}\gamma_{j,TO}\omega} \tag{1}$$

where Ω_j and γ_j are, respectively, the resonant frequency and damping factor of the jth longitudinal (subscript LO) or transversal (subscript TO) optical mode. The width of the jth mode is directly related to the corresponding damping factor γ_j.

The high-limit value ε_∞ of the dielectric function has been deduced from the optical refraction index ($n = \sqrt{\varepsilon_\infty}$). The ordinary ($n_0$, E$_\mathrm{u}$ symmetry) and extraordinary (n_e, A$_\mathrm{u}$ symmetry) optical indices [18] were controlled with a Pulfrich-refractometer.

Table 6. Frequencies of transverse and longitudinal infrared-active phonons in lithium fluoride scheelites LiLnF$_4$ (Ln = Ho, Er, Tm, Yb; Y).

	$LiYF_4$					$LiTmF_4$			$LiTbF_4$
Mode (cm^{-1})	This work (300 K)	Schulteiss *et al* [16] (330 K)	Miller *et al* [13] (77 K)	$LiHoF_4$	$LiErF_4$	This work (300 K)	Kupchikov *et al* [15]	$LiYbF_4$	Dörfler *et al* [24]
A_u	196/219	192/229	195/224	196/220	196/219.5	196/220	206/215	191/217	202/221
(TO/LO)	251/278	255/287	252/283	232/261	230/261	232/264	238/262	228/263	239/262
	241/360	404/464	396/—	340/368	339/361	343/367	352/364	344/368	347/353
	370/534	489/—	490/—	369/516	375/516	372/519	382/—	377/520	369/529
E_u	137/171	144/186	143/173	135/168	136/170	137/171	142/174	139/174	142/165
(TO/LO)	294/308	262/276	293/303	277/302	278/302	278/303	282/302	277/302	281/298
	325/367	314/372	326/367	321/349	320/350	321/349	323/340	315/343	319/345
	418/560	413/556	424/566	418/553	420/554	424/557	415/—	419/555	431/556

Table 6 lists the frequencies of LO and TO modes used to obtain the best fit reflectivity curves (full curves in figure 4), which are in a good agreement with experimental ones (dotted curves). Typically, LO and TO frequencies are determined to better than 2 cm^{-1} for low frequencies, and better than 5 cm^{-1} over 300 cm^{-1}. Note that the oscillator strength $\Delta\varepsilon_j$ of the jth transversal mode can be directly deduced from the LO/TO splittings through the relation:

$$\Delta\varepsilon_j = \frac{\varepsilon_\infty}{\Omega^2_{j,\mathrm{TO}}} * \frac{\prod_k(\Omega^2_{k,\mathrm{LO}} - \Omega^2_{k,\mathrm{TO}})}{\prod_{k\neq j}(\Omega^2_{k,\mathrm{TO}} - \Omega^2_{j,\mathrm{TO}})}.$$

Transverse- and longitudinal-mode profiles are given by the imaginary part of the dielectric and inverse dielectric functions which are reported for the reference compound $LiYF_4$ in figures 5(a) ($E//c$) and (b) ($E\perp c$). Surprisingly, only the second band of each polarization is dependent on the trivalent ion nature (Y or Ln). The corresponding A_u and E_u frequencies are lowered by about 15 cm^{-1}, which may indicate a global motion of the LnF$_8$ (YF$_8$) entity. The lowest-frequency optical A_u and E_u modes, not affected by the Y/Ln substitution, therefore do not imply significant motions of the trivalent ion.

From our data, it is possible to deduce the optical indices and the absorption coefficient:

$$n(\omega) = \left(\frac{1}{2}\sqrt{\varepsilon'^2 + \varepsilon''^2} + \frac{\varepsilon'}{2}\right)^{1/2}$$
$$k(\omega) = \left(\frac{1}{2}\sqrt{\varepsilon'^2 + \varepsilon''^2} - \frac{\varepsilon'}{2}\right)^{1/2}$$
$$\alpha(\omega) = 2\omega k(\omega)/c.$$

The curves $n(\omega)$ and $k(\omega)$ are of course of interest for the optical applications of these materials; they are reported in figure 6 ($E//c$ and $E\perp c$) for all of the compounds studied in this work. The frequency dependence of the absorption coefficient is illustrated in figure 5(c) for the reference compound $LiYF_4$.

The discrepancy between the results of Miller or Schulteiss (also reported in table 6) and ours is simple to understand: absorption measurements lead to the overestimation of TO frequencies in highly damped modes since the absorption maximum does not then coincide with the TO frequency.

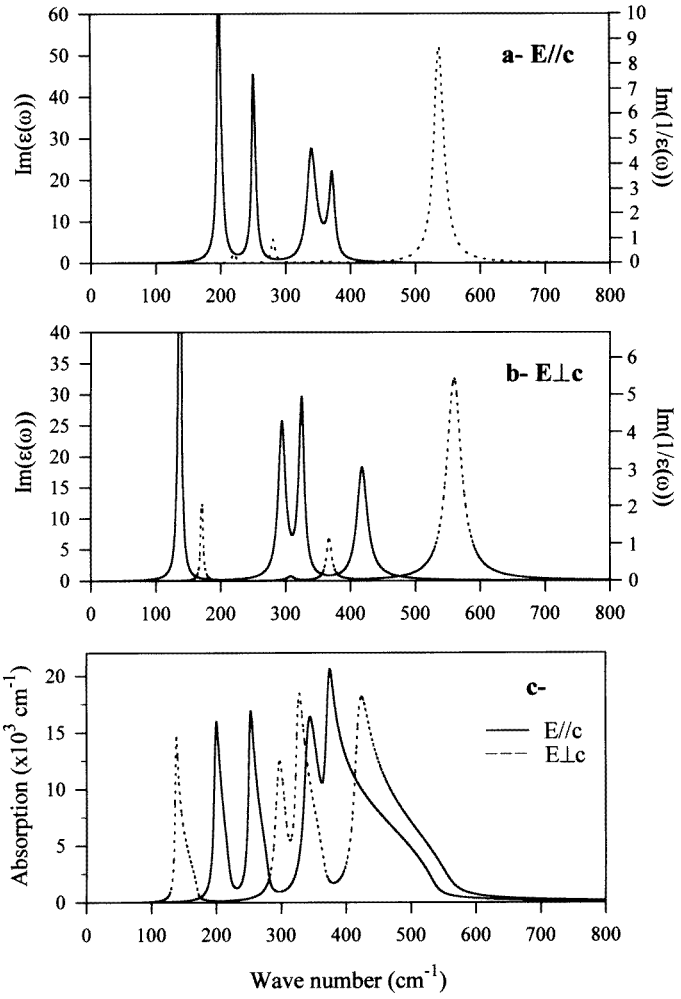

Figure 5. Calculated frequency dependent functions in $LiYF_4$. (*a*) and (*b*) Transverse and longitudinal modes profiles given by the imaginary part of the dielectric function ($\mathrm{Im}(\varepsilon(\omega))$, full curves), and inverse dielectric function ($\mathrm{Im}(1/\varepsilon(\omega))$, dotted lines) respectively, for $E//c$ (*a*) and $E\perp c$ (*b*). (*c*) Absorption coefficient $\alpha(\omega)$.

4.3. Effective charges

The knowledge of $\varepsilon(\omega)$ enables the calculation of the ionic effective charges Ze, defined by Scott [25], which are related to the LO/TO splitting for polyatomic systems through the following relation:

$$\sum_j (\Omega^2_{j,\mathrm{LO}} - \Omega^2_{j,\mathrm{TO}})_\alpha = \frac{1}{V\varepsilon_V} \sum_k \frac{(Ze)^2_{k\alpha}}{M_k}.$$

The sums are done on the modes (index j) for the left part, and on the atoms (index k) for the right part. α refers to the polarization direction, V is the volume of the unit cell, and M_k is the mass of the corresponding k ion.

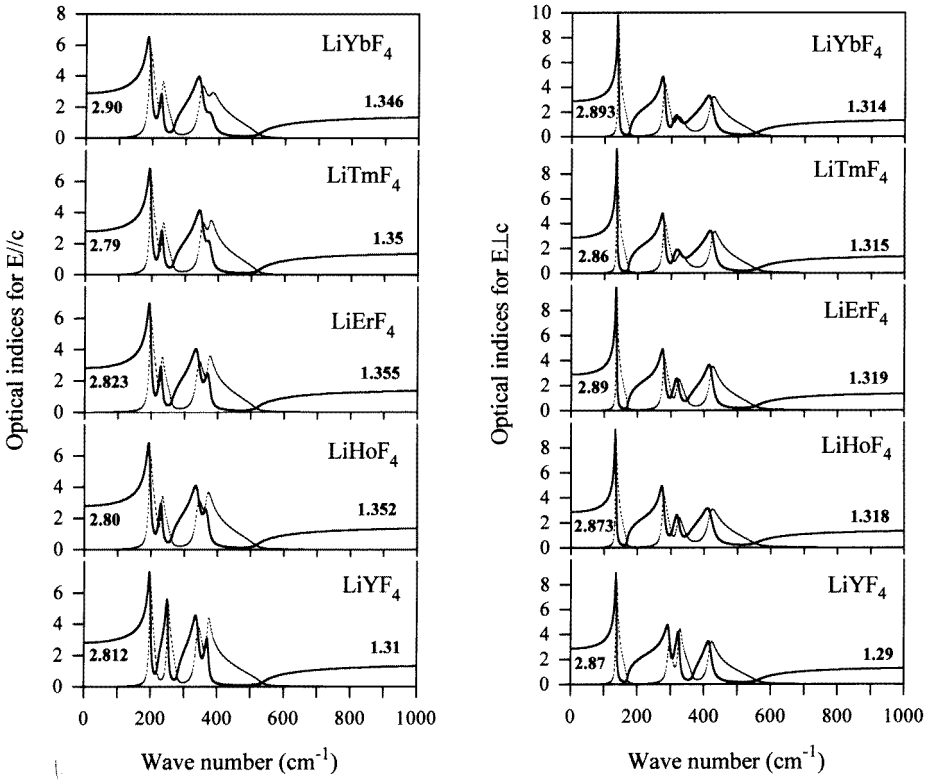

Figure 6. Calculated refraction index $n(\omega)$ (full curve) and extinction index $k(\omega)$ (dotted curve) in lithium fluoride scheelites LiLnF$_4$(Ln = Ho, Er, Tm, Yb; Y).

In the LiLnF$_4$ compounds, there are only two equations (previous formula and electrical neutrality of the crystal) but three different effective charges have to be determined. Therefore, it appears necessary to fix one of the charges. It seems to be convenient to impose the lithium effective charge since several self-consistent data have been obtained for this particular ion, namely:

- Z(Li) = 0.72 (obtained in the binary crystal LiF [26])
- Z(Li) = 0.6 (in the ternary compound BaLiF$_3$ [27])
- Z(Li) = 0.65 (intermediate case).

The corresponding charges of the fluorine and lanthanide ions are reported in table 7.

We also present in table 7 the resulting charges when choosing for the lanthanide ion the effective charge obtained in the LaF$_3$ compound. The infrared data [28] used to obtain this charge are well-suited only for the polarization perpendicular to the optical axis (namely E$_u$ modes). The frequencies of the A$_u$ modes in LaF$_3$ are indeed not so precise as E$_u$ ones because the spectra they were deduced from have been recorded without any light polarization.

All these effective charges may seem questionable in so far as they depend on the choice of one of the charges. Nonetheless, the results we obtain are quite self consistent. The $(Ze)^2/M$ ratios in the above relation which relates the LO/TO splitting to the effective charges, are indeed very different; the main components are those of lithium (because of its small mass) and fluorine (heavier than Li$^+$ but with a contribution four times larger due to

Table 7. Effective charges (in units of $|e|$) for polar A_u and E_u modes calculated on the basis of the measured LO/TO splittings in LiLnF$_4$ fluoride scheelites (Ln = Ho, Er, Tm, Yb; Y).

		$LiYF_4$		$LiHoF_4$		$LiErF_4$		$LiTmF_4$		$LiYbF_4$	
		A_u	E_u	A_u	E_u	A_u	E_u	A_u	E_u	A_u	E_u
Z(Li) = 0.72	Z(F)	−0.8	−0.79	−0.80	−0.82	−0.80	−0.82	−0.79	−0.81	−0.80	−0.82
	Z(Ln)	2.48	2.44	2.47	2.56	2.46	2.55	2.44	2.52	2.50	2.54
Z(Li) = 0.65	Z(F)	−0.82	−0.81	−0.82	−0.84	−0.82	−0.84	−0.81	−0.83	−0.83	−0.84
	Z(Ln)	2.62	2.58	2.64	2.72	2.63	2.72	2.61	2.69	2.66	2.71
Z(Li) = 0.60	Z(F)	−0.83	−0.82	−0.84	−0.86	−0.84	−0.86	−0.83	−0.85	−0.84	−0.86
	Z(Ln)	2.71	2.67	2.75	2.83	2.75	2.83	2.72	2.80	2.78	2.83
$Z(Ln)$ = 2.656	Z(F)	—	−0.82	—	−0.83	—	−0.83	—	−0.83	—	−0.83
	Z(Li)	—	0.61	—	0.68	—	0.68	—	0.66	—	0.67

the number of fluorine ions in the crystalline motive). The ratio which corresponds to an Ln ion is so small when compared with the previous ones that a great variation of $Z(Ln)$ barely influences other ionic charges.

Moreover, the calculated effective charge of fluorine ions is very close to those deduced in other fluoride compounds such as perovskites [27, 29–31]. This is in agreement with the strong ionic character of bonds which imply fluorine ions. In addition, we observe that the fluorine effective charge is very weakly affected by the variations of Z(Li) or $Z(Ln)$: the fluorine seem to be 'shared' equally between Li and Ln ions. Finally, we may also point out that the effective charge of the Ln ions stay roughly constant in the whole LiLnF$_4$ series of compounds.

5. Conclusion

IR and Raman active modes have been measured in $LiYF_4$ and LiLnF$_4$ compounds (Ln = Ho, Er, Tm and Yb) and assigned to the various irreducible representations of the point group of the crystal. The study of the laser-matrix $LiYF_4$ has yielded the frequencies of three modes (lowest A_g and two higher A_u (LO) modes) which had not been shown by previous studies. The results about $LiYF_4$ have been used as a reference for the interpretation of Raman spectra of the LiLnF$_4$ in which electronic Raman effect and luminescence are also observed. The measured electronic Raman lines, evidenced in low temperature LiLnF$_4$ Raman spectra for Ln = Tm, Ho and Yb, are in a good agreement with the calculated differences of energy between crystal-field levels of LSJ states (with respect to the selection rules), and with the results obtained by other authors. One may also note that the frequency dependence of the optical indices n and k have been deduced from the IR measurements, these particular curves being a useful tool for the optical studies that may be conducted in any compound of the LiLnF$_4$ series.

For each compound, all of the phonon modes set in the frequency range 0–500 cm^{-1}. As previously shown by Miller *et al* [13], we cannot separate the internal vibrations of the LiF_4^{3-} unit from external vibrations in fluoride scheelites unlike in oxides, because these compounds are highly ionic in character. Nonetheless, the comparison between the frequencies obtained in $LiYF_4$ and LiLnF$_4$ compounds brings some informations about the atomic motions. Indeed, an Ln^{3+} ion being about twice as heavy as Y^{3+}, the frequencies of modes that

imply movements of trivalent ions (potentially E_g, E_u, B_g and A_u modes) should decrease from $LiYF_4$ to $LiLnF_4$. Raman results are in agreement with those considerations: the two lowest-frequency modes of each E_g and B_g symmetries are lowered when replacing Y by an Ln^{3+} ion. Concerning IR measurements, only the position of the second band, which frequency (in each polarization) is lowered by about 15 cm^{-1}, is affected by the substitution of a lanthanide ion to yttrium. These particular two A_u and E_u modes therefore certainly imply much more important movements of A^{3+} ions than the lowest and highest ones. Nonetheless, only lattice dynamical calculations, based on Raman, infrared and inelastic neutron scattering data, can yield reliable information about real atomic displacements induced by phonon modes. This kind of work has been realised in the reference compound $LiYF_4$ and is reported in paper II.

References

[1] Thoma R E, Brunton G D, Penneman R E and Keenan T K 1970 *Inorganic Chemistry* **9** 1096
[2] Keller C and Schmutz H 1965 *J. Inorg. Nucl. Chem.* **27** 900
[3] Thoma R E, Wearer C F, Insley H, Harris L A and Yarkel H A Jr 1961 *J. Phys. C: Solid State Phys.* **65** 1096
[4] Kaminskii A 1990 *Laser Crystals* (Berlin: Springer)
[5] Christensen H P 1979 *Phys. Rev.* B **19** 6564
[6] Christensen H P 1979 *Phys. Rev.* B **19** 6573
[7] Rubin J, Brenier A, Moncorgé R and Pedrini C 1986 *J. Lumin.* **36** 39
[8] Brenier A, Rubin J, Moncorgé R and Pedrini C 1989 *J. Physique* **50** 1463
[9] Rubin J, Brenier A, Moncorgé R and Pedrini C 1987 *J. Physique* **48** 1761
[10] Petrov M V, Tkachuk A M and Feofilov P P 1981 *Izv. AN. SSSR Ser. Fiz.* **45** 3
[11] Harmer A L, Linz A and Gabbe D R 1969 *J. Phys. C: Solid State Phys.* **30** 1483
[12] Meichenin D, Auzel F, Hubert S, Simoni E, Louis M and Gesland J Y 1994 *Electron. Lett.* **30** 1309
[13] Miller S A, Rast H E and Caspers H H 1970 *J. Chem. Phys*. **52** 4172
[14] Korableva S L, Kupchikov A K, Petrova M A and Ryskin A J 1980 (Engl. transl.) *Sov. Phys.–Solid State* **22** 1115
[15] Kupchikov A K, Malkin B Z, Rzaev D A and Ryskin A I 1982 *Sov. Phys.–Solid State* **24** 1348
[16] Schulteiss E, Scharmann A and Schwabe D 1986 *Phys. Status Solidi* b **138** 465
[17] Garcia E and Ryan R R 1993 *Acta Crystallogr.* C **49** 2053
[18] Landolt-Börnstein 1973 *Numerical Data and Functional Relationships in Science and Technology* vol 7 (Berlin: Springer)
[19] Shannon R D 1976 *Acta Crystallogr.* A **32** 751
[20] Barker A S Jr 1964 *Phys. Rev.* **135** 742
[21] Porto S P S and Scott J F 1967 *Phys. Rev.* **157** 716
[22] Kupchikov A K, Malkin B K, Natadze A L and Ryskin A I 1987 *Sov. Phys.–Solid State* **29** 1913
[23] Kiel A and Porto S P S 1969 *J. Mol. Spectrosc.* **32** 458
[24] Dörfler W 1984 *Thesis* University of Würzburg
[25] Scott J F 1971 *Phys. Rev.* B **4** 1360
[26] Catlow C R A, Diller K M and Norgett M J 1977 *J. Phys. C: Solid State Phys.* **10** 395
[27] Boumriche A, Simon P, Rousseau M, Gesland J Y and Gervais F 1989 *J. Phys.: Condens. Matter* **1** 5613
[28] Rast H E, Caspers H H, Miller S A and Buchanan R A 1968 *Phys. Rev.* **171** 1051
[29] Ridou C, Rousseau M and Gervais F 1986 *J. Phys. C: Solid State Phys.* **19** 5757
[30] Salaün S, Mortier M, Gesland J Y, Rousseau M and Hennion B 1993 *J. Phys.: Condens. Matter* **5** 7615
[31] Salaün S and Rousseau M 1995 *Phys. Rev.* B **51** 15 867 and references therein